Preliminary Evaluation of Altitude Scaling for Turbofan Engine Ice Crystal Icing

Jen-Ching Tsao*
Ohio Aerospace Institute, Cleveland, OH 44142

This paper presents some preliminary evaluation results of a full turbofan engine ice crystal icing altitude scaling application for a heavily instrumented ALF502R-5 engine test conducted in the NASA Glenn Research Center Propulsion Systems Laboratory (PSL) during October and November of 2015. This engine, S/N LF11, was instrumented with four internal video cameras to observe various ice buildup processes downstream of the second exit guide vane trailing edge (i.e. EGV2 TE) region of the low pressure compressor (LPC). To determine possible scale test conditions at lower altitudes a reference condition chosen from one of this engine's key rollback test points, i.e. FLT 850, was selected. The scaling method considered is based on the thermodynamic model developed previously to describe the potential ice accretion on unheated surfaces inside a turbofan engine compression system from fully glaciated ice crystal clouds. The PSL engine icing test capability has been demonstrated in its 2013 inaugural ice crystal icing test. But the rather limited ice crystal cloud calibration range available at the time and the lack of reliable measurement instrumentation needed along the internal core flow passage of the LPC has prevented one to setup the desired local airflow and ingested ice crystal cloud thermal and phase conditions according to the scaling method. Consequently a simplified altitude scaling approach was investigated. The NASA in-house engine icing risk assessment code COMDES was utilized to determine possible scale test conditions at lower altitude with similar engine icing risk potential by best matching the following three icing related parameters of the reference condition: (1) the local air static wet bulb temperature and (2) the local ice crystal melt ratio of a prescribed smaller particle size at the EGV2 trailing edge location, and (3) the engine fan face total water content to air density ratio of the ice crystal cloud. The instantaneous images and the time-lapsed movies of ice buildup in the EGV2 TE region were acquired in LF11 and are used with other relevant air and ice crystal thermodynamic and engine performance data to assess the lower altitude icing simulation results. It is found from the preliminary evaluation that altitude scaling is possible in PSL to simulate the important ice crystal accretion features and the associated icing effects on engine performance.

Nomenclature

b, b^*	=	Modified relative heat factor, dimensionless
c, c^*	=	Specific ratio of ice particle kinetic heating to latent heat absorbed from melting, dimensionless
$c_{p,air}$	=	Specific heat of air, cal/g K
$c_{p,ws}$	=	Specific heat of water at the surface temperature, cal/g K
h_c	=	Convective heat-transfer coefficient, cal/s m^2 K
h_G	=	Gas-phase mass-transfer coefficient, g /s m^2
h_G	=	Gas-phase mass-transfer coefficient, g /s m^2
IWC	=	Ice water content, g/m^3
IWAR	=	Non-dimensional ice water content, = IWC/ρ_a
LWC	=	Liquid water content of melted ice, g/ m^3
MR	=	Ice crystal melt ratio, = LWC_t/IWC_i, dimensionless
M_∞	=	Local Mach number, dimensionless
MMD	=	Ice crystal median mass diameter, μm
MVD	=	Water droplet median volume diameter, μm
N1	=	Fan speed, rpm
N2	=	Core speed, rpm

* Principal Research Scientist, 21000 Brookpark Rd., MS 11-2, AIAA Associate Fellow.

$\dot{m}_e$ = mass flux of water evaporated per unit time, lbm/ft^2 s
$\dot{m}_{imp}$, = mass flux of ice/liquid-water particle impinged per unit time, lbm/ft^2 s
$\dot{m}_{melt,imp}$ = mass flux of water-melt impinged per unit time, lbm/ft^2 s
m_0 = Stagnation melting fraction, dimensionless
n_0 = Stagnation freezing fraction, dimensionless
p = Pressure, N/m^2
p_w = Vapor pressure of water in atmosphere, N/m^2
p_{ww} = Vapor pressure of water at the icing surface, N/m^2
q_{conv} = Surface heat loss due to convection, Btu/hr ft^2
q_{evap} = Surface heat loss from evaporation, Btu/hr ft^2
q_{freeze} = Surface heat gain from release of latent heat of fusion, Btu/hr ft^2
$q_{kinetic}$ = Surface heat gain from kinetic energy of ice crystals and water drops, Btu/hr ft^2
q_{melt} = Surface heat loss from release of latent heat of fusion, Btu/hr ft^2
RH = Relative humidity, dimensionless
RTD1 = Total air temperature in the test section when cloud on
SH = Specific humidity, g of water vapor/kg of dry air
T_f = Freezing temperature of bulk water, °C
T_{ice} = Ice crystal temperature, °C
T_{melt} = Water melt temperature, °C
T_s = Icing surface temperature, °C
T_{wall} = Wall temperature, °C
T_∞ = Air static temperature, °C
V = Air velocity, kt
VWC_{gain} = Vapor water content gained (i.e. = $VWC_t - VWC_i$) , g/ m^3
W = Fan face mass flow rate, lbm/s
β_0 = Collection efficiency at stagnation line, dimensionless
ϕ = Ice/water mass energy transfer parameter, °C
Λ_f, Λ_v = Latent heat of freezing and condensation, cal/g
θ = Air/vapor energy transfer parameter, °C
ρ_a = Air density, kg/m^3

Subscripts

cor = corrected
ff = fan face
i = inlet, initial or dry condition
pl = in the plenum
t = target, terminal or wet condition
s = at the surface
0 = stagnation value
1 = PSL-3 contraction duct exit plane, i.e. station 1
∞ = local static condition

I. Introduction

Many turbofan engine power-loss events have been observed since 1990 on both commuter and large transport aircraft near large deep convective weather systems at high altitudes[1]. The deep convective updraft core can bring a large amount of condensed water from the surface to the cloud top. The predicted maximum ice water content (IWC) above the freezing level could reach up to about 9 g/m^3 in theory[2] at around 30,000 ft. In addition, from more recent High Altitude Ice Crystals (HAIC)/High Ice Water Content (HIWC) flight campaign measurement data[3] available on microphysical properties of deep convective clouds it appeared that at cold temperature levels (-40°C or below), high IWC areas are primarily composed of small ice crystals (200-400 μm), which yield small MMDs around 300 μm. This suggests that high IWC regions at high altitudes occur in and above young convective regions where small ice crystal are nucleated in large quantities.

Based on the instrumented flight-testing data collected in commuter and transport aircraft engine events, Mason *et al.*[1] has proposed a hypothesis for possible ice accretion due to ice crystal ingestion. The hypothesis recognizes

that ice crystals could begin to melt causing mixed-phase conditions within the compression system passage of the engine. This mixed-phase water mass would impinge and accrete on unheated surfaces within the engine where the local air temperature was significantly higher than freezing before entering the cloud. This ice crystal icing inside the engine core flowpath has been shown to create flow blockage leading to loss of thrust and hardware damage due to shedding. The hypothesis specifically stated that liquid water is a necessary condition locally for ice accretion to continue. Furthermore, it was believed that this ice crystal accretion phenomenon is not unique only to commuter or transport aircraft engine type and therefore it was expected that certain common physical mechanisms for ice crystal accretion on all jet engines should exist.

To better understand the fundamental aspects of ice crystal accretion physics and possible influence of high concentrations of ice crystals on engine performance and operability, NASA and National Research Council Canada collaborated on a series of fundamental icing physics experimental studies[4,5,6,7] to examine possible physical mechanisms of ice accretion on surfaces exposed to fully glaciated ice crystal and mixed-phase conditions similar to those believed to be encountered during engine power-loss events.

Key findings from those early studies included: **(1)** the air wet bulb temperature, T_{wb}, was identified to be an effective parameter to represent the air/water vapor mixture (i.e. humid air) temperature for studying ice-crystal icing process, **(2)** the ice crystal cloud melt ratio, *MR*, was also identified as an important parameter for the onset and actual growth rate of ice-crystal accretion, **(3)** the ingested amount of IWC was considered a critical parameter directly affecting the possible onset and the ice growth rate and **(4)** there are two distinct types of ice crystal accretion observed on an unheated icing surface: (i) when the "*surface freezing fraction"* is positive, it is dominated by the freezing of water melt from fully or partially melted ice crystals, the ice structure is formed from accretion with strong adhesion to the surface and little water runback, and (ii) when the "*surface melting fraction"* is positive, it is dominated by the further melting of ice crystals, the ice structure is formed from accumulation of un-melted ice crystals with relatively weak bonding to the surface and lots of visible surface water runback.

In 2013 the first NASA ice crystal engine icing test was conducted[8] on an unmodified ALF502R-5 engine, S/N LF01, which was flown during Honeywell's 1997 flight test campaign[9]. This test has shown that the PSL, though using the NASA Icing Research Tunnel (IRT) spray bar system technology, was able to successfully replicate several known in-flight engine icing events (including the FLT 850 full rollback) and non-rollback events as well. By developing such a ground based altitude ice crystal icing simulation facility, detailed aero and thermodynamic profiles of the humid air and ingested ice/water particle size, mass and phase distribution measurement data inside the engine core flow path region can be obtained to enable researchers to better understand the underlying physical mechanisms in order to further improve and validate the existing in-house engine icing simulation and risk prediction codes.[10,11,12,13,14] These engineering modeling tools will be available to the U.S. aviation community to help assess the potential icing risks and ice protection system requirement as an acceptable Means of Compliance (MOC) for icing design and certification purpose.

In NASA's current research plan to address the technical challenge of engine icing for the N+2/ N+3 design concepts there is a milestone to develop an adequate icing scaling method for full engine near sea-level testing which is advantageous from a cost saving consideration because altitude facilities are expensive and time consuming to operate. The altitude scaling for ice crystal icing is a condition scaling method used to determine the scale test conditions which would reproduce the same ice shape from the reference condition. Recently a new thermodynamic model was developed[15] specifically for engine ice crystal icing phenomenon, and the model analysis has been examined with aforementioned fundamental ice crystal icing physics experimental data[4,5] and with selected data from the 2013 full scale ALF 502-R5 LF01 turbofan engine ice crystal icing test[8.] The preliminary results showed that the model is able to capture important qualitative trends of the ice crystal ice formation observed in the engine second exit guide vane (EGV2) region under different icing conditions. This model has become the theoretical base of new altitude scaling method development[16]. The focus of this study is to show some preliminary evaluation results of the proposed altitude scaling method from this heavily instrumented ALF502-R5 LF11 engine icing test[17,18] conducted in PSL in 2015.

II. Proposed Similarity Parameters for Engine Ice Crystal Icing Scaling Application

This aforementioned thermodynamic model for engine ice crystal icing (ICI) was primarily based on the scaling work originally done by Ruff[19] and later extended by Anderson[20] and Anderson and Tsao[21] using the Messinger's[22] steady-state surface energy balance analysis for super-cooled liquid water icing in both Appendix C and super-cooled large droplet (SLD) regimes. The expressions for the parameters used will be presented here without much discussion. Therefore, readers who are interested in the physical descriptions and detailed derivations of these parameters are referred to Ref. 19 and 20 and the references given therein. Several key modifications were made to

the surface energy balance equation in order to account for possible interactions between the local air flow within the low pressure compressor flow passage and the ingested ice crystals from the engine inlet.

A. Model Assumptions

Currently the model only considers the engine ice crystal icing phenomenon for a fully glaciated ice crystal cloud which is the most prevalent cloud characteristic in or around a large deep convective weather system at high altitudes[1]. Figure 1 depicts the notional schematics of ice crystal particle path through the ALF502-R5 engine inlet, the fan-core rotor and stator (inlet guide vane - IGV), the low pressure compressor (LPC) rotor (supercharger) and tandem stators (EGV1, EGV2), the gooseneck duct and the support strut. When the surface energy balance analysis is applied at the stagnation region of a LPC component, the model assumes or considers:

- local air flow is steady relative to accretion process,
- accretion is quasi-steady,
- fully glaciated ice particle cloud with single particle size,
- no LWC supplement (i.e. fully glaciated ice crystal cloud at inlet),
- when ice particles experience some melting, $T_{ice} = T_{melt} = T_f$ (i.e. $0 < MR < 1$),
- when MR = 0 (no melting), $T_{ice,\,i} < T_{ice} < T_f$,
- when MR = 1 (fully melted), $T_f < T_{melt} < T_0$,
- for partially-melted ice particle cloud, $LWC_t = IWC_i * MR$, $IWC_t = [IWC_i * (1 - MR)] - VWC_{gain}$,
- on unheated surface (T_{wall} could be fairly hot initially),

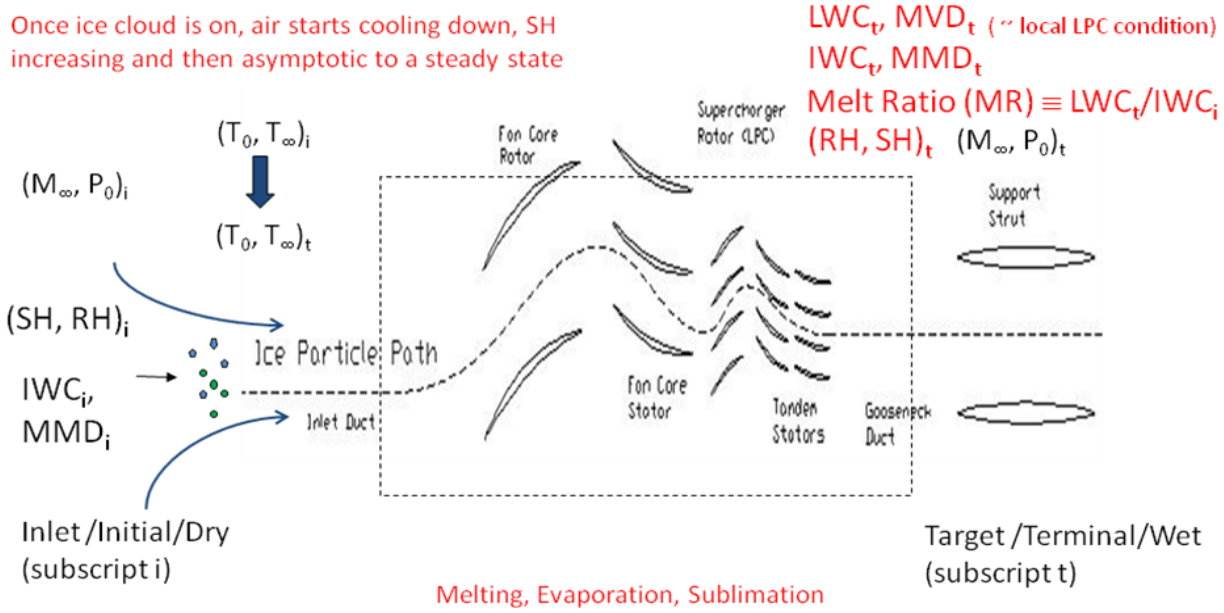

Figure 1. The schematics of ice particle path through an engine fan and LPC region.

- $T_s = T_f$ when glaze ice accreted or accumulated on surfaces.

B. The Surface Energy Balance Equation

As duly noted in Ref. 4 & 5, there are two distinct types of ice growth mechanism in ice crystal icing. For the sake of brevity, only the final equations and key expressions of parameters are presented without much discussion. These two types of ice growth mechanism are described as follows:

(1) <u>Freezing dominated process on surface when cooling > heating</u> (i.e. $0 \le n_0 \le 1$)

$$q_{conv} + q_{evap} - q_{kinetic} = q_{freeze} \tag{1}$$

where

$$q_{conv} = h_c (T_s - T_\infty - V_\infty^2 / 2c_{p,air}),$$

$$q_{evap} = \dot{m}_e L_v = h_G \frac{\left(\left[\frac{p_{v,ws}}{T_\infty} - \left(\frac{P_0}{T_0} \right) \frac{p_{v,w\infty}}{P_\infty} (RH) \right] \right)}{\frac{1}{0.622} \left(\frac{P_0}{T_0} \right) - \left(\frac{p_{v,ws}}{T_\infty} \right)} \Lambda_v,$$

$$q_{kinetic} = \dot{m}_{imp,t} \frac{(V_\infty)^2}{2} = (IWC_i - VWC_{gain}) * \beta_0 * V_\infty * (1 - n_{loss})_0 * \frac{(V_\infty)^2}{2},$$

$$q_{freeze} = \dot{m}_{melt,imp} * n_0 * \Lambda_f = (IWC_i * MR * \beta_0 * V_\infty) * (1 - n_{loss})_0 * n_0 * \Lambda_f.$$

Substituting the expressions for various heat flux terms listed above into Eqn. (1) it can be rewritten in the following form

$$n_0 = \left(\frac{c_{p,ws}}{(MR) * \Lambda_f} \right) \left(\frac{IWC_i - VWC_{gain}}{IWC_i} \right) \left(\phi + \frac{\theta_0}{b_0} \right) \tag{2}$$

The freezing fraction is formally defined as the ratio of the amount of water that freezes at a given surface location to the total amount of water that impinges at that location. The key terms in this formulation include ϕ and θ_0, which have dimensions of temperature and relate to the ice/water mass energy transfer and air/vapor energy transfer, and b_0, the relative heat factor, which was first introduced by Tribus, *et al*.[23]

$$\phi = \left(-\frac{V_\infty^2}{2c_{p,ws}} \right),$$

$$\theta_0 = \left(T_s - T_\infty - \frac{V_\infty^2}{2c_{p,air}} \right) + \frac{h_G}{h_c} \left[\frac{\frac{p_{v,ws}}{T_\infty} - \left(\frac{P_0}{T_0} \right) \frac{p_{v,w\infty}}{P_\infty} (R.H.)}{\frac{1}{0.622} \left(\frac{P_0}{T_0} \right) - \left(\frac{p_{v,ws}}{T_\infty} \right)} \right] \Lambda_v,$$

$$b_0 = \left(\frac{\dot{m}_{imp,t} c_{p,ws}}{h_c} \right) = \frac{(IWC_i - VWC_{gain}) * \beta_0 * (1 - n_{loss})_0 * V_\infty * c_{p,ws}}{h_c}.$$

With some algebraic manipulations, Eq. (2) can be further expressed as

$$n_0 = \frac{1}{b_0^*} (T_s - T_{wb,0}) - c_0^* \tag{3}$$

in which $T_{wb,0}$ denotes the total air wet bulb temperature and is given as

$$T_{wb,0} = \left(T_\infty + \frac{V_\infty^2}{2c_{p,air}} \right) - \frac{h_G}{h_c} \left[\frac{\frac{p_{v,ws}}{T_\infty} - \left(\frac{P_0}{T_0} \right) \frac{p_{v,w\infty}}{P_\infty} (R.H.)}{\frac{1}{0.622} \left(\frac{P_0}{T_0} \right) - \left(\frac{p_{v,ws}}{T_\infty} \right)} \right] \Lambda_v,$$

and

$$b_0^* = b_0\left(\frac{(MR)\Lambda_f}{Cp_w}\right)\left(\frac{IWC_i}{IWC_i - VWC_{gain}}\right) = \frac{\dot{m}_{imp}(MR)\Lambda_f}{h_c}\left(\frac{IWC_i/\rho_a}{\left(IWC_i - VWC_{gain}/\rho_a\right)}\right),$$

$$c_0^* = \left(\frac{V_\infty^2/2}{(MR)\Lambda_f}\right)\left(\frac{IWC - VWC_{gaini}}{IWC_i}\right) = \left(\frac{\left(\frac{\gamma}{2}RT_\infty\right)M_\infty^2}{(MR)\Lambda_f}\right)\left(\frac{IWC_i/\rho_a}{\left(IWC_i - VWC_{gain}\right)/\rho_a}\right).$$

From Eq. (3), it is apparent that both parameters $T_{wb,0}$ and *MR* can affect the accretion process but they are not unique. There are many combinations of $T_{wb,0}$ and *MR* that lead to the same freezing fraction n_0. It is also noted that for a given local thermal profile, i.e. fixed $T_{wb,0}$ and *MR*, the freezing fraction n_0 decreases as (IWC_i/ρ_a) increases. This non-dimensional term (IWC_i/ρ_a) suggests that for engine icing problem the air density compressibility effect via altitude pressure is also important. For the same amount of IWC_i ingested by the engine, the local effective IWC value, (IWC/ρ_a), becomes larger with decreasing density due to increasing altitude. This effect was first noticed and reported by Veres[24] *et al*. in their recent engine icing analysis work in terms of the ice-water flow rate to air flow rate ratio, ***IWAR,*** from this heavily instrumented LF11 engine icing test data.

This clearly suggests that the most important parameter affecting the ice crystal accretion process is the freezing fraction n_0 which is a function of (IWC_i/ρ_a), $T_{wb,0}$ and *MR*.

(2) <u>Melting dominated process on surface when heating > cooling</u> (i.e. $0 \le m_0 \le 1$)

$$q_{kinetic} - q_{conv} - q_{evap} = q_{melt} \tag{4}$$

Carrying out the similar substitution procedure as described above, Eq. (4) can be rewritten as

$$m_0 = \frac{MR}{b_0^*\left(1 - MR - \left(\frac{VWC_{gain}}{IWC_i}\right)\right)}(T_{wb,0} - T_s) + \frac{MR}{\left(1 - MR - \left(\frac{VWC_{gain}}{IWC_i}\right)\right)}c_0^* \tag{5}$$

Similar to the freezing dominated process, Eq. (5) also shows that for melting dominated process on icing surfaces both parameters $T_{wb,0}$ and *MR* can affect the resulting ice accumulation structure through the melting fraction m_0 but they are not unique. In addition, for a given $T_{wb,0}$ and *MR*, the surface ice growth and size (before ice shedding occurs) will increase as (IWC_i/ρ_a) is increased while the melting fraction m_0 decreases.

III. Scaling Method Evaluation from LF11 Engine Icing Test Data

NASA PSL Ice Crystal Icing Heavily Instrumented Engine Test

As shown from Eq. (3) and (5), for possible similarity of ice crystal accretion on specific unheated surface location within the engine LPC system flow passage, it is necessary for the scale test to simulate the geometry, the flowfield, the ice/water particle trajectories, the total water catch, the heat transfer and, probably, the surface phenomena of the desired reference icing condition. However most of the needed information to conduct proper scaling calculation for this LF11 engine were not available at the time. Thus an alternative approach to find potential scale test conditions was established as follows:

(1) The FLT 850 case EGV2 icing condition was chosen as the reference condition for this scaling study,

(2) A number of scale test conditions, with similar engine ICI risk at an altitude of 5,000 ft (5k ft) with best matching engine fan-core and LPC operation characteristics (ex: the engine fan face Mach number M_{ff}, the corrected engine fan face mass flow rate W_{cor}, and the corrected engine fan rotational speed $N1_{cor}$) from FLT 850, were calculated with NASA in-house codes COMDES[24] and MELT by matching the following three icing parameters of the reference condition at the EGV2 trailing edge and fan face locations:

   a. the local static wet bulb temperature $T_{wb,\infty}$
   b. the local melt ratio ($MR_{EGV2,\,TE}$) of a prescribed smaller ice particle size (i.e. 5 μm) and

c. the engine fan face ***IWAR*** of the ice crystal cloud (i.e. the non-dimensional ice water content ≡ IWC/ρ_a). Ideally, it should match the local ***IWAR*** if the information or measurements of particle size redistribution over the supercharger rotor (see Figure 1) were available.

(3) A parametric sweep of IWC, MMD, N1 and T_{pl} around each proposed scale condition will be performed (within the facility operation limit) to ensure sufficient coverage of local reference icing conditions at EGV2 trailing edge would be simulated to allow reasonable evaluation of such proposed scaling method.

It should be noted that the PSL engine icing test cell continues working on improving its ability to have better icing cloud quality in terms of cloud uniformity. The in-house codes are still under development and are very much limited by the current state of art capability in instrumentation and measurement to acquire high quality local physical variable data inside the engine compression system for ice crystal icing simulation verification and validation. In addition, there is no safe and easy close-up visual access to engine LPC exit guide vanes near shroud leading edge regions where early ice accretion and shedding were taking place. With those constraints in mind, the images and the time-lapsed movies of how the ice structure was formed in the downstream area of EGV2 trailing edge along the outer shroud casing surface represent the only available visual characterization of resulting ice accretion. The qualitative comparison of ice formation allows one to visually evaluate how closely this simplified altitude scaling approach could simulate the reference ice crystal accretion features.

A. The Reference and Scale Test Conditions

The actual run conditions of the reference case (Rdg 93) and two 5k ft scale test cases (Rdg 406 and Rdg 416) chosen for comparison are listed as follows in Table 1.

Table 1. The reference FLT 850 and two 5k ft scale test conditions in 2015 PSL LF11 engine icing test

PSL ESCORT DATA								COMDES/MELT OUTPUT								
Escort Rdg#	Alt (kft)	$N1^*$	M_{amb}	T_{amb} (°C)	T^*_{pl}	IWC_1 (g/m³)	MMD_1 (μm)	M^*_{ff}	IWAR	$T_{wbs,\ EGV2\ TE}$ (°C)	$T_{surf,\ EGV2,\ 20s,\ avg}$ (°C)	MR EGV2 TE	RH EGV2 TE (%)	W^*_{cor}	$N1^*_{cor}$	CRB
93	28.9	1.00	0.52	-30.0	1.000	2.3	23	1.00	5.05	-1.32	2.96	0	7.9	1.00	1.06	Y (69s)
406	4.89	0.95	0.19	-20.8	0.994	5.4	24	1.05	4.51	-1.48	3.68	0	10.6	1.03	1.01	N (close)
416	4.86	0.95	0.19	-26.4	0.971	6.4	18	1.07	5.19	-5.26	1.79	0	10.0	1.05	1.02	Y (393s)
		*			*			*						*	*	

Noted in this table that (1) the first eight columns are the PSL designated run number and seven specific measurement data output from PSL Escort data system, (2) the next eight columns represent calculated quantities obtained from COMDES and MELT codes and (3) the last column shows the net icing effect (i.e. rollback (RB) or not) on this engine and the time taken to call a rollback (CRB). In addition some quantities highlighted with * symbols were further normalized by the corresponding reference values, e.g. the engine actual and corrected fan speed ($N1^*$, $N1^*_{cor}$), the PSL plenum air total temperature (T^*_{pl}), the engine fan face Mach number (M^*_{ff}) and the corrected fan face mass flow rate (W^*_{cor}).

B. The Reference and Scale Test Fan-core and LPC Operation Comparison

In identifying the possible scale test conditions at lower altitudes special attention was given to those with similar engine fan-core and LPC operation characteristics to the reference FLT 850 setting. It was noticed from the table that although the physical ambient Mach number and fan speed are different, both scale test cases do have similar normalized fan face Mach number, the corrected fan speed and the corrected fan face mass flow rate as the reference case for this LF11 engine. Furthermore Figure 2 which is a standard engine fan-core/LPC characteristic performance plot also shows that the engine LPC operation setting was fairly close between the reference and those two 5k ft scale test cases.

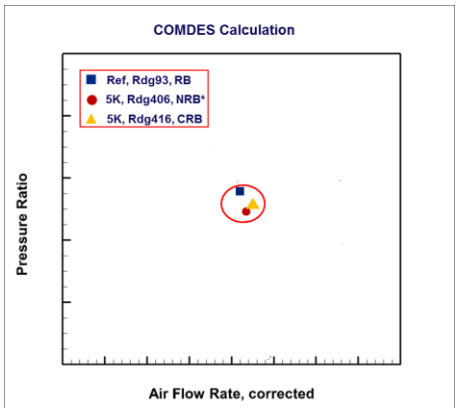

Figure 2. The LF11 engine fan-core and LPC performance calculation points for the reference FLT 850 and those two 5k ft scale test conditions

C. The Reference and Scale Test ICI Simulation Comparison

As stated in the beginning of this section, the 5k ft scale test conditions should match the local static wet bulb temperature and the local melt ratio of smaller ice particle of 5 μm size at the EGV2 trailing edge (TE) location, and the engine fan face ***IWAR*** value of the reference condition to ensure a similar engine ice crystal icing risk based on the well calibrated 1-D COMDES code calculation for this engine. However this does not guarantee a similar ice accretion growth at the EGV2 TE location and a similar simulation of icing effect on the engine performance since the COMDES code currently still does not have a way yet to account for important leading order effects from larger ice particle impact, mixed phase ice particle and icing surface interaction, surface runback and surface convective heat transfer characteristics. Thus a parametric sweep of IWC, MMD, N1 and T_{pl} around each proposed scale condition will be performed (within the facility operation limit) to ensure sufficient coverage (i.e. the key is to capture the minimum IWC threshold from NRB to RB or vice versa) of local reference icing conditions at the EGV2 trailing edge would be simulated. This could provide us some useful information (besides matching ***IWAR***) regarding how the scale IWC value at the lower altitude testing should be scaled from the reference IWC value.

(1) Rdg 93 vs Rdg 406

Figure 3 depicts a sequence of ice buildup images on the EGV2 TE outer shroud surface area for the reference FLT 850 case. The time-lapsed movie suggests the local ice accretion captured by the internal cameras is a melting-dominated ice formation process with frequent ice shedding of varying intensity. It should be noted that the reference IWC value of 2.3 g/m^3 has exceeded the minimum IWC threshold needed for a RB event to occur.

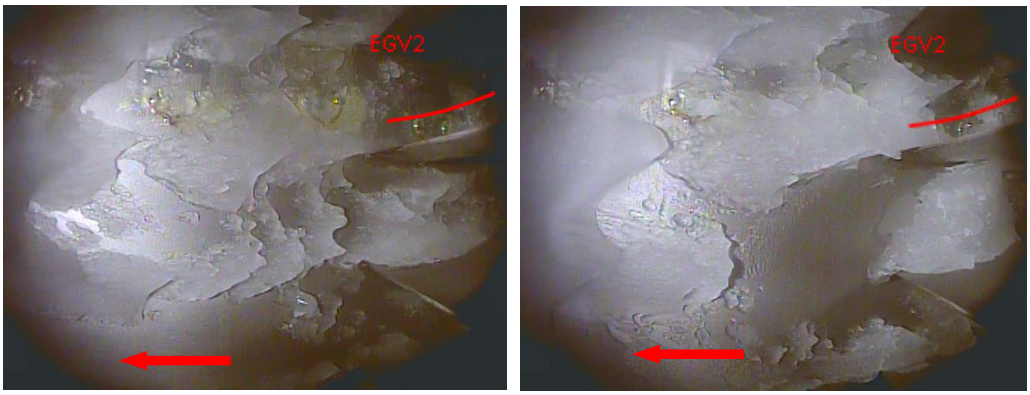

Figure 3. Two ice buildup images on the EGV2 TE outer shroud area captured by the internal cameras for the reference FLT 850 case. The time progresses from left to right image, and the flow direction in each image is moving from right to left.

Figure 4 shows another sequence of ice buildup images on the EGV2 TE outer shroud surface area for the 5k ft scale test case Rdg 406. The time-lapsed movie suggests the local ice accretion is also a melting-dominated ice

formation process with similar reference local static wet bulb temperature and melt ratio. However it became obvious during the post data analysis that the scale test IWC value of 5.4 g/m^3 did not exceed the minimum IWC threshold needed for a reference like RB event to occur at this altitude. Judging from the EGV2 surface metal thermal couple (TC) reading average value over the spray time and the ice shedding frequency and intensity it was estimated that if the scale IWC could increase by 20-30% or more, a CRB event with similar reference ice growth features would occur. This is an expected tradeoff in using this 1-D COMDES code, though heavily calibrated by the engine icing test data, to identify similar engine icing risk conditions at different altitudes for scaling evaluation. It still needs a relatively wider range of IWC to ensure the scale condition sweep would capture (or surround) the target reference icing condition conservatively. However for this scale test condition the IWC sweep clearly did not go large enough.

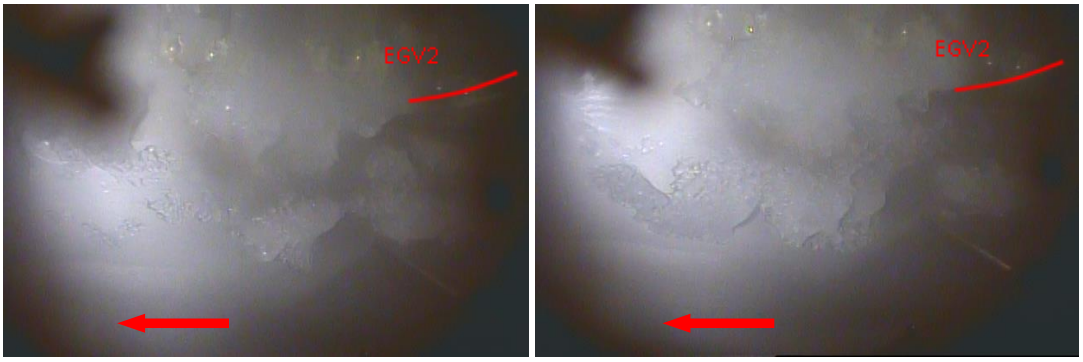

Figure 4. Two ice buildup images on the EGV2 TE outer shroud area captured by the internal cameras for the 5k ft scale test case Rdg 406. The time progresses from left to right image, and the flow direction in each image is moving from right to left.

After this test point, the LF11 engine icing test team decided to drop the plenum air temperature T_{pl} by 5 °C to conduct another similar parametric sweep to see whether a RB event could occur.

(2) <u>Rdg 416</u>

Figure 5 displays a couple of ice buildup images in time for this new 5k ft scale test anchor point Rdg 416. The time-lapsed movie clearly shows that at this colder static wet bulb temperature and near freezing EGV2 metal surface temperature the local ice accretion becomes a freezing-dominated ice formation process with firmer ice sheet buildup and less frequent ice shedding. This simulated icing event was occurring at a slower rate of thrust reduction even with a much larger scale IWC value of 6.4 g/m^3 (about 20% more than Rdg 406 case). This suggests a higher minimum IWC threshold is required for a RB event to occur in this freezing-dominated regime like the Rdg 416.case.

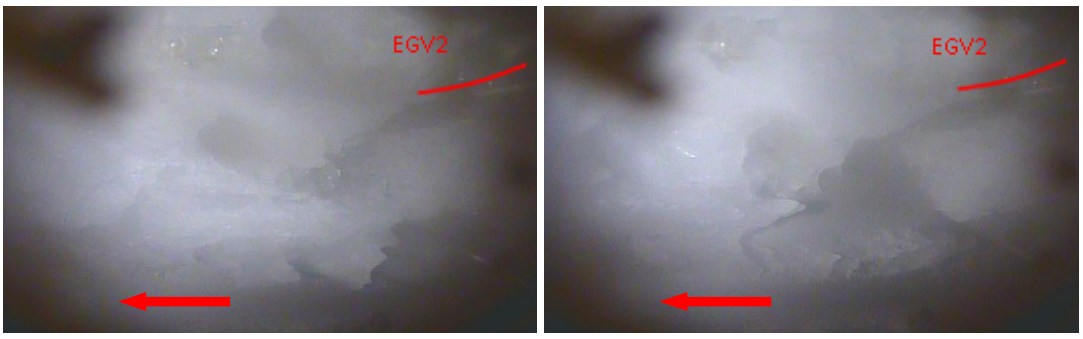

Figure 5. Two time sequences of ice buildup image on the EGV2 TE downstream shroud area captured by the internal cameras for the 5k ft scale test case Rdg 416. The time sequence progresses from left to right, and the flow direction is moving from right to left.

D. The Reference and Scale Test ICI Engine Response Simulation Comparison

The reference Rdg 93 case is a full RB simulation of FLT 850 field event in PSL with this heavily instrumented LF11 engine. Figures 6-8 show three selected time sequences of ice buildup images along the EGV2 TE outer shroud surface area and the corresponding engine responses[17] (load, fan and core speeds, booster EGV average metal surface temperatures) during this full RB simulation. Noted that the engine response plots shown here also have included the comparison with the LF01 engine full RB point Rdg 193 obtained from the 2013 inaugural engine ice crystal icing test campaign. For readers who are interested in how ice crystal icing can impact this LF11 engine performance they are referred to Refs. 17 and 18 for more details. After some careful examination of those figures,

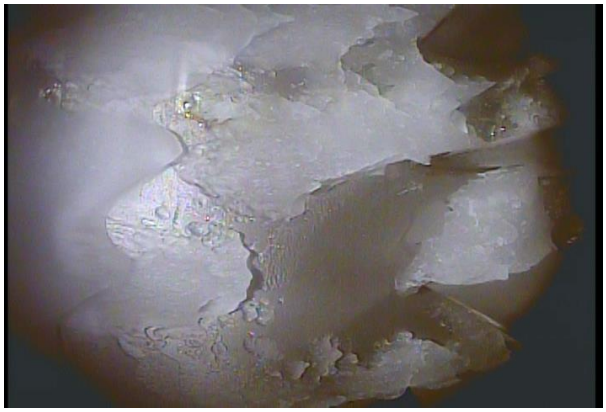

Figure 6(a). Ice buildup at sequence 1

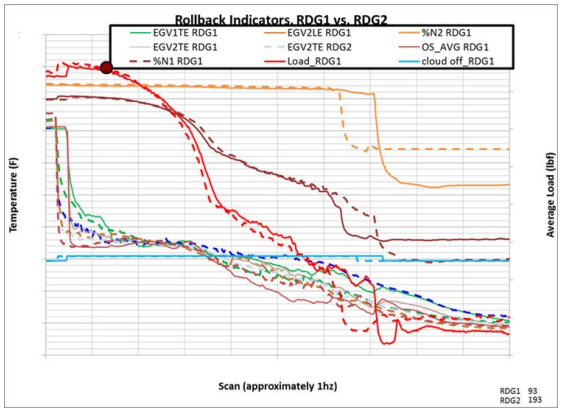

Figure 6(b). Engine response at sequence 1

Figure 7(a). Ice buildup at sequence 2

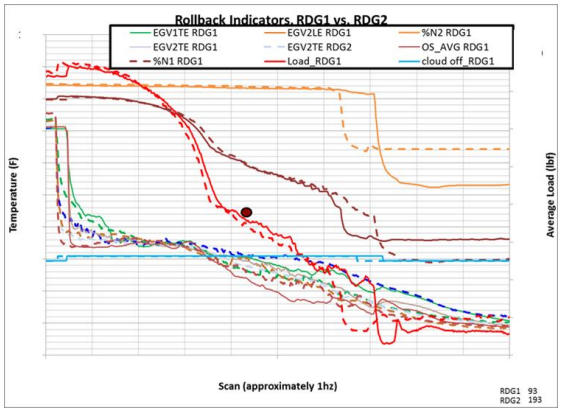

Figure 7(b). Engine response at sequence 2

Figure 8(a). Ice buildup at sequence 3

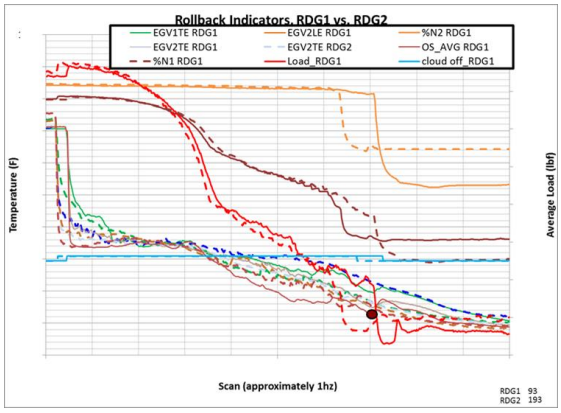

Figure 8(b). Engine response at sequence 3

it becomes apparent that the view captured is not of high value to the scaling method evaluation. Clearly the ice buildup on the outer shroud alone could not explain the engine performance degradation seen from those figures. There are other critical ice accretion processes hidden away from the camera. Therefore it is imperative to develop a better ice shape characterization method to help one understand what critical ice shape features at critical locations (could be challenging to have access though) impact the engine performance the most since not all ice accretion types pose engine risk.

As for those two selected 5k ft scale test cases, i.e. Rdg 406 and 416, they were all run and evaluated in a called rollback mode. Consequently, there are no detailed comparison of engine response simulation could be made for them with the reference Rdg 93 case. A rather simple called rollback (CRB) or no rollback (NRB) and the time to CRB were used to assess how well this simplified scaling approach could be used to simulate the reference engine response from ICI. The Rdg 406 case was a NRB with a reference like ICI accretion feature. However the scale IWC value used was not large enough to have a CRB. As for the Rdg 416 case, it was a CRB, but it was different from the reference FLT 850 case. It had a firmer ice sheet buildup and infrequent ice shedding which led to a slower rate of thrust reduction and a larger minimum IWC threshold needed for a freezing-dominated RB to occur. As a simple comparison, the CRB time for Rdg 416 case is nearly six times longer than the reference Rdg 93 case.

IV. Conclusion

A simplified approach for altitude scaling consideration has been evaluated for the 2015 LF11 engine icing test campaign conducted in the NASA Glenn Research Center Propulsion Systems Laboratory. This approach first utilizes a LF01/LF11 calibrated NASA in-house engine icing risk assessment code COMDES to determine possible scale test conditions at 5k ft altitude with similar engine ICI risk by matching the following three icing parameters of the reference condition at the EGV2 trailing edge location while maintaining similar fan-core and LPC operation characteristics as the reference :

(1) the local air static wet bulb temperature,
(2) the local ice crystal melt ratio of a prescribed smaller ice particle of 5 μm size, and
(3) the engine fan face ***IWAR*** value of the ice crystal cloud.

A parametric sweep of IWC, MMD, N1 and T_{pl} around each 5k ft scale condition was performed to better understand both the ice accretion and the engine icing effect characteristics. This would help evaluate how similarly the reference ICI and engine icing effect features being simulated.

The instantaneous images and the time-lapsed movies of ice buildup in the EGV2 TE region could only provide limited ICI accretion characteristic information. A better ice shape characterization method with respect to the ice shape effects on engine is clearly needed. Those ice buildup images on the engine EGV2 outer shroud area are used with other relevant air/ice crystal thermodynamic and engine performance data to qualitatively and visually assess the 5k ft engine ICI simulation results. It is found from the preliminary evaluation that altitude scaling is possible for PSL or a sea level engine test facility to simulate the important ice crystal accretion features and the associated ICI effects on engine performance. But special considerations and unique test methods are needed in order to address the associated facility operation limitations, e.g. altitude vs sea level or direct connect vs blow through test facility, for running different type of engine icing test configurations, for example a full engine vs a motor driven rig.

Acknowledgments

The author wishes to acknowledge the financial support for this work by the Advanced Air Transport Technologies (AATT) project under NASA's Advanced Air Vehicles Program (AAVP). This work is in response to the Engine Icing Technical Challenge. Special thanks are extended to AAI subproject manager Mr. Anthony Nerone and the NASA Icing Branch Chief Mrs. Mary Wadel for their support of the work. The author also wishes to acknowledge the help and guidance received from Mr. Joe Veres and Dr. Philip Jorgenson for providing the general flow simulation of the LF11 engine system from the Honeywell Engines customer deck (CD) and the COMDES/MELT code spreadsheet.

References

[1] Mason, J.G., Strapp, J.W. and Chow, P., "The Ice Particle Threat to Engines in Flight," AIAA-2006-0206, January 2006.

[2] Mazzawy, R. S. and Strapp, J.W., "Appendix D – An Interim Icing Envelope," *SAE 2007 Aircraft and Engine*

Icing International Conference, 2007-01-3311

[3] Leroy, D., Coutris, P., Emmanuel, F., Schwarzenboeck, A., Strapp, J., Lilie, L. and et al., "HAIC/HIWC Field Campaigns – Specific Findings on Ice Crystals Characteristics in High Ice Water Content Cloud Regions," *8th AIAA Atmospheric and Space Environments Conference*, AIAA-2016-4056, 2016

[4] Struk, P., Currie, T., Wright, W. B., Knezevici, D. C., Fuleki, D., Broeren, A., Vargas, M. and Tsao, J. C., "Fundamental Ice Crystal Accretion Physics Studies," SAE 2011 International Conference on Aircraft and Engine Icing and Ground Deicing, SAE 2011-38-0018, June 2011

[5] Currie, T. C., Struk, P. M., Tsao, J. C., Fuleki, D. and Knezevici, D. C., "Fundamental Study of Mixed-Phase Icing with Application to Ice Crystal Accretion in Aircraft Jet Engines," AIAA-2012-3035, June 2012

6Currie, T., Fuleki, D., Knezevici, D., and MacLeod, J., "Altitude Scaling of Ice Crystal Accretion," AIAA-2013-2677, June 2013

[7] Currie, T. C., Fuleki, D., and Mahallati, A. "Experimental Studies of Mixed-Phase Sticking Efficiency for Ice Crystal Accretion in Jet Engines," *6th AIAA Atmospheric and Space Environments Conference*, AIAA-2014-3049, 2014

[8] Oliver, M. J. "Validation Ice Crystal Icing Engine Test in the Propulsion Systems Laboratory at NASA Glenn Research Center," *6th AIAA Atmospheric and Space Environments Conference*, Atlanta, GA, June 16-20, 2014, AIAA-2014-2898.

[9] Goodwin, R.V., Dischinger, D.G., "Turbofan Ice Crystal Rollback Investigation and Preparations Leading to Inaugural Ice Crystal Engine Test at NASA PSL-3 Facility," *6th AIAA Atmospheric and Space Environments Conference*, Atlanta, GA, June 16-20, 2014, AIAA-2014-2895.

[10] Bidwell, C., "Ice Particle Transport Analysis with Phase Change for the E^3 Turbofan Engine Using LEWICE3D Version 3.2," *4th AIAA Atmospheric and Space Environments Conference*, New Orleans, LA, June 25-28, 2012, AIAA-2012-3037.

[11] Bidwell, C., "Ice Particle Analysis of the Honeywell ALF502 Engine Booster," *SAE 2015 International Conference on Aircraft and Engine Icing and Ground Deicing,* 2015-01-2131

[12] Rigby, D. and Bidwell, C., "Three Dimensional Navier-Stokes Simulation of Flow in an Axial Low Pressure Compressor at Engine Icing Operation Conditions," *SAE 2015 International Conference on Aircraft and Engine Icing and Ground Deicing,* 2015-01-0139

[13] Veres, J. P., Jorgenson, P. C. E., "Modeling Commercial Turbofan Engine Icing Risk with Ice Crystal Ingestion," *5th AIAA Atmospheric and Space Environments Conference,* San Diego, CA, June 24-27, 2013, AIAA 2013-2679 and NASA/TM-2013-218097

[14] Veres, J.P., Jones, S.M., Jorgenson, P.C.E., "Performance Modeling of Honeywell Turbofan Engine Tested with Ice Crystal Ingestion in the NASA Propulsion System Laboratory," *SAE 2015 International Conference on Aircraft and Engine Icing and Ground Deicing,* 2015-01-2133

[15] Tsao, J., Struk, P. M., and Oliver, M. J., "Possible Mechanisms for Turbofan Engine Ice Crystal Icing at High Altitude," *6th AIAA Atmospheric and Space Environments Conference*, AIAA-2014-3044, 2014.

[16] Struk, P. M., Bencic, T., Tsao, J.C., Fuleki, D. and Knezevici, D.C., "Preparation for Ice-Crystal Icing Scaling Studies at the NRC Research Altitude Test Facility," AIAA-2013-2675, June 2013

[17] Flegel, A. B. and Oliver, M. J., "Preliminary Results from a Heavily Instrumented Engine Ice Crystal Icing Test in a Ground Based Altitude Test Facility," *8th AIAA Atmospheric and Space Environments Conference*, AIAA-2016-3894, 2016

[18] Goodwin, R. V. and Fuleki, D., "Engine Preparation and Instrumentation for the Second Ice Crystal Engine Test at NASA PSL-3 Test Facility," *8th AIAA Atmospheric and Space Environments Conference*, AIAA-2016-3892,

2016.

[19] Ruff, G.A., "Analysis and Verification of the Icing Scaling Equations," AEDC-TR-85-30, vol 1 (rev), March 1986.

[20] Anderson, D. N., "Manual of Scaling Methods," NASA /CR–2004-212875, March 2004.

[21] Anderson, D. N. and Tsao, J. C., "Ice Shape Scaling for Aircraft in SLD Conditions," NASA/CR-2008-215302, DOT/FAA/AR-07/55, September 2008.

[22] Messinger, B.L., "Equilibrium Temperature of an Unheated Icing Surface as a Function of Airspeed," *J. Aeron. Sci.*, vol. 20 no. 1, January 1953, pp 29 – 42.

[23] Tribus, Myron, Young, G.B.W. and Boelter, L.M.K., "Analysis of Heat Transfer Over a Small Cylinder in Icing Conditions on Mount Washington," *Trans. ASME*, vol. 70, November 1948, pp 971 – 976.

[24] Veres, J. P., Jorgenson, P. C. E. and Jones, S. M., "Modeling of Highly Instrumented Honeywell Turbofan engine Tested with Ice Crystal Ingestion in the NASA Propulsion System Laboratory," 8th AIAA Atmospheric and Space Environments Conference, AIAA-2016-3895, 2016.